The Astronomical Journal, 168:66 (11pp), 2024 August https://doi.org/10.3847/1538-3881/ad4b16

Discovery of the Remarkably Red L/T Transition Object VHS J183135.58-551355.9

Thomas P. Bickle[1], Adam C. Schneider[2], Jonathan Gagné[3,4], Jacqueline K. Faherty[5], Austin Rothermich[5], Johanna M. Vos[5,6], Genaro Suárez[5], J. Davy Kirkpatrick[7], Aaron M. Meisner[8], Marc J. Kuchner[9], Adam J. Burgasser[10], Federico Marocco[7], Sarah L. Casewell[11], Dan Caselden[5], and Daniella C. Bardalez Gagliuffi[12]
The Backyard Worlds: Planet 9 Collaboration

[1] School of Physical Sciences, The Open University, Milton Keynes, MK7 6AA, UK; tombickleastro@outlook.com
[2] United States Naval Observatory, Flagstaff Station, 10391 West Naval Observatory Road, Flagstaff, AZ 86005, USA
[3] Planétarium de Montréal, Espace pour la Vie, 4801 av. Pierre-de Coubertin, Montréal, QC, H1V 3V4, Canada
[4] Trottier Institute for Research on Exoplanets, Université de Montréal, Département de Physique, C.P. 6128 Succ. Centre-ville, Montréal, QC, H3C 3J7, Canada
[5] Department of Astrophysics, American Museum of Natural History, Central Park West at 79th Street, NY 10024, USA
[6] School of Physics, Trinity College Dublin, The University of Dublin, Dublin 2, Ireland
[7] IPAC, Mail Code 100-22, Caltech, 1200 E. California Boulevard, Pasadena, CA 91125, USA
[8] NSF's National Optical-Infrared Astronomy Research Laboratory, 950 N. Cherry Avenue, Tucson, AZ 85719, USA
[9] Exoplanets and Stellar Astrophysics Laboratory, NASA Goddard Space Flight Center, 8800 Greenbelt Road, Greenbelt, MD 20771, USA
[10] Department of Astronomy & Astrophysics, University of California San Diego, La Jolla, CA 92093, USA
[11] School of Physics and Astronomy, University of Leicester, Leicester, LE1 7RH, UK
[12] Department of Physics & Astronomy, Amherst College, 25 East Drive, Amherst, MA 01003, USA
Received 2024 April 1; revised 2024 May 4; accepted 2024 May 6; published 2024 July 9

Abstract

We present the discovery of VHS J183135.58−551355.9 (hereafter VHS J1831−5513), an L/T transition dwarf identified as a result of its unusually red near-infrared colors ($J - K_S = 3.633 \pm 0.277$ mag; $J - W2 = 6.249 \pm 0.245$ mag) from the VISTA Hemisphere Survey and CatWISE2020 surveys. We obtain low-resolution near-infrared spectroscopy of VHS J1831−5513 using the Magellan Folded port InfraRed Echellette spectrograph to confirm its extremely red nature and assess features sensitive to surface gravity (i.e., youth). Its near-infrared spectrum shows multiple CH_4 absorption features, indicating an exceptionally low effective temperature for its spectral type. Based on proper-motion measurements from CatWISE2020 and a photometric distance derived from its K_s-band magnitude, we find that VHS J1831−5513 is a likely (∼85% probability) kinematic member of the β Pictoris moving group. Future radial velocity and trigonometric parallax measurements will clarify such membership. Follow-up mid-infrared or higher-resolution near-infrared spectroscopy of this object will allow for further investigation as to the cause(s) of its redness, such as youth, clouds, and viewing geometry.

Unified Astronomy Thesaurus concepts: Brown dwarfs (185); L dwarfs (894); T dwarfs (1679); Stellar associations (1582); Moving clusters (1076)

Materials only available in the online version of record: data behind figure

1. Introduction

At young ages, brown dwarfs have not yet contracted to their final equilibrium radii (Burrows et al. 1997) and have low masses for their effective temperatures. They therefore have lower surface gravities and lower-pressure atmospheres than their field-age counterparts. This low pressure reduces collision-induced absorption (CIA) by H_2 (Linsky 1969; Borysow et al. 1997) and it is hypothesized that it causes an excess of clouds and dust in their photospheres (Cushing et al. 2008; Faherty et al. 2016), shifting emergent flux to longer wavelengths (e.g., Faherty et al. 2012). Consequently, the near-infrared colors of young brown dwarfs are notably redder than those of field-age objects of the same spectral type (Faherty et al. 2016; Liu et al. 2016).

Young, red L and T dwarfs can act as valuable analogs for young, giant exoplanets, possessing similar effective temperatures, masses, and atmospheric properties (Liu et al. 2013; Faherty et al. 2016). The planets HR8799 bcde (Marois et al. 2008, 2010) and planetary-mass companions VHS 1256−1257 b (Gauza et al. 2010), 2M1207 b (Chauvin et al. 2004), and BD +60 1417 b (Faherty et al. 2021) are apt examples of this, all exhibiting near-infrared spectra consistent with red, low-gravity, late-L dwarfs. Crucially, young free-floating substellar objects can be studied without the interference of light from a host star, providing convenient and effective laboratories for tests of planetary theory (Faherty et al. 2016). This convenience does, however, come at a cost; whereas companions can have properties (e.g., age and metallicity) inferred from their host star under the assumption of common formation, the properties of free-floating brown dwarfs are notoriously difficult to determine. An age–mass–temperature degeneracy exists for brown dwarfs (Burrows et al. 1997), making it challenging to pinpoint these three key properties for isolated brown dwarfs. However, if a brown dwarf can be linked through kinematics and age diagnostics to a known moving group with a well-constrained age, this degeneracy inherent in brown dwarfs can be broken, and properties consistent throughout that group's membership, such as age (e.g., Bell et al. 2015) and metallicity (e.g., Viana Almeida et al. 2009), may be attributed to the object. When the age of an object is inferred, evolutionary models can be used to estimate physical properties such as mass and effective temperature (e.g., Filippazzo et al. 2015; Suárez et al. 2021). Such objects are vital

benchmarks for studying brown dwarf evolution, and at young ages and low masses can provide important empirical constraints to the initial mass function (Gagné et al. 2017; Kirkpatrick et al. 2021, 2024).

While targeted searches using the Two Micron All-Sky Survey (2MASS; Skrutskie et al. 2006) have discovered unusually red, nearby L dwarfs (Kellogg et al. 2015; Schneider et al. 2017), the detection limit of 2MASS ($J \approx 17$ mag) means that many low-mass, red L/T dwarfs are missed. This restriction is the primary reason that the number of spectroscopically confirmed free-floating L/T dwarfs with extremely red colors ($J - K > 2.2$ mag) remains low ($\sim$15). The advent of a new generation of surveys, such as the VISTA Hemisphere Survey (VHS; McMahon et al. 2013), the UKIDSS Large Area Survey (UKIDSS LAS; Lawrence et al. 2007), and UKIRT Hemisphere Survey (UHS; Dye et al. 2018), which probe significantly deeper than 2MASS (5σ J-band depths of 20.2, 19.9, and 19.6 mag, respectively), has brought the potential for the discovery of objects with fainter J-band magnitudes than previously possible (e.g., Schneider et al. 2023a). Consequently, these surveys are ideal hunting grounds for young, red L and T dwarfs, the J bands of which are inherently suppressed. Reaching fainter J-band magnitudes also means that redder objects than previously known have become detectable. Indeed, until Schneider et al.'s (2023a) discovery of the reddest known free-floating L/T dwarf CWISE J050626.96+073842.4 (CWISE J0506+0738; $(J-K)_{\rm MKO} = 2.974 \pm 0.039$ mag) using UHS, it had been approximately a decade since the discovery of the previously reddest known objects PSO J318.5338−22.8603 ($(J-K)_{\rm MKO} = 2.74 \pm 0.04$ mag; Liu et al. 2013) and ULAS J222711−004547 ($(J-K)_{\rm MKO} = 2.79 \pm 0.06$ mag; Marocco et al. 2014). The discovery of such extraordinarily red objects is important as it allows us to explore parameters that influence the appearance of brown dwarfs such as youth, metallicity, clouds, and viewing inclination (e.g., Looper et al. 2008; Vos et al. 2017; Suárez & Metchev 2022, 2023). It is also vital for understanding the differences between free-floating planetary-mass objects and directly imaged exoplanets. Directly imaged exoplanets occupy a unique color–magnitude sequence (e.g., Gratton et al. 2024), and the discovery of extremely red, faint objects such as CWISE J0506+0738 (a strong candidate member of the β Pictoris moving group, or BPMG; Schneider et al. 2023a), serves to narrow the color–magnitude gap.

In this work, we present VHS J183135.58−551355.9 (hereafter VHS J1831−5513), an L/T transition dwarf with anomalously red near-infrared colors. At $J - K_{\rm S} = 3.633 \pm 0.277$ mag, it is potentially the reddest known free-floating substellar object, more so than the current reddest spectroscopically confirmed object in the literature, CWISE J0506+0738, by $\sim$0.66 mag. In Section 2, we discuss the discovery of VHS J1831−5513. In Section 3, we present Magellan/The Folded port InfraRed Echellette (FIRE) spectroscopic follow-up data, and in Section 4, we analyze and discuss those data. In Section 5, we evaluate young moving group membership, estimate physical properties, and investigate the prospects for variability in VHS J1831−5513.

2. Identification of VHS J1831–5513

The unique color space occupied by young L dwarfs makes it possible to perform targeted searches using a photometric approach: a particularly valuable property given their typically low tangential velocities (Faherty et al. 2009, 2012), which makes their discovery through proper-motion-based searches (e.g., Backyard Worlds; Kuchner et al. 2017; Humphreys et al. 2020) challenging. Utilizing this principle, we performed a half-sky search of CatWISE2020 (CatWISE; Marocco et al. 2021) and VHS for objects with extremely red ($J - K_{\rm S} > 2$ mag, $J - W2 > 4$ mag) near-infrared colors (T. Bickle et al. 2024, in preparation). VHS J1831−5513 was discovered during a secondary search, which used the CatWISE reject table instead of the main CatWISE catalog, in order to collect any spuriously rejected candidates. VHS J1831−5513 was rejected by CatWISE due to the overlap of a latent (a.k.a. charge persistence; Eisenhardt et al. 2020) artifact in the Wide-field Infrared Survey Explorer (WISE). We used WiseView (Caselden et al. 2018), a tool designed to aid the visualization of motion in WISE time-resolved coadds, to vet VHS J1831−5513, and confirmed the presence of an overlapping latent.[13] We therefore checked the unTimely catalog (Kiwy 2022; Meisner et al. 2023) to investigate if its CatWISE photometry was adversely affected. This showed that both the W1 and W2 bands were affected by $\sim$0.1−0.2 mag in the scan direction where the latent was present, but both to a similar extent, so while the CatWISE W1–W2 color is not completely unaffected, it is approximately accurate, with an offset from the average unTimely W1–W2 color in the epochs where the latent is absent of only 0.012 mag. We also visually inspected the higher-resolution VHS imagery to confirm there were no obvious contaminants or resolved companions affecting its near-infrared colors. Once these checks were complete, and we were satisfied that VHS J1831−5513 was a genuine extremely red candidate, it was added to our list for follow-up spectroscopy. The CatWISE2020 and VHS photometry for VHS J1831−5513 are presented in Table 1.

Table 1
Properties of VHS J1831−5513

Parameter	Value	References
α [J2000] (deg)	277.898262	(1)
δ [J2000] (deg)	−55.232219	(1)
μ_α[a] (mas yr^{-1})	1.43 ± 9.6	(2)
μ_δ[a] (mas yr^{-1})	−84.24 ± 10.4	(2)
J (mag)	20.175 ± 0.229	(1)
$K_{\rm S}$ (mag)	16.542 ± 0.048	(1)
W1 (mag)	14.735 ± 0.018	(2)
W2 (mag)	13.926 ± 0.016	(2)
$d_{\rm phot}$[b] (pc)	55.4 ± 5.5	(3)
Spectral type (NIR)	L8γ–T0γ	(3)

Notes.
[a] Proper-motion values corrected for CatWISE2020 systematic offsets.
[b] Photometric distance estimated using the VHS $K_{\rm S}$ magnitude and the absolute magnitude–spectral type relation of Dupuy & Liu (2012).
References: (1) VHS DR6 (McMahon et al. 2013); (2) CatWISE2020 Reject Table (Marocco et al. 2021); (3) This work.

3. Observations

We used the 6.5 m Magellan Baade telescope and the FIRE spectrograph (Simcoe et al. 2013) to obtain near-infrared spectra for VHS J1831−5513. Observations were made on 2023 June 30 under clear conditions. We operated FIRE in the

[13] http://byw.tools/wiseview

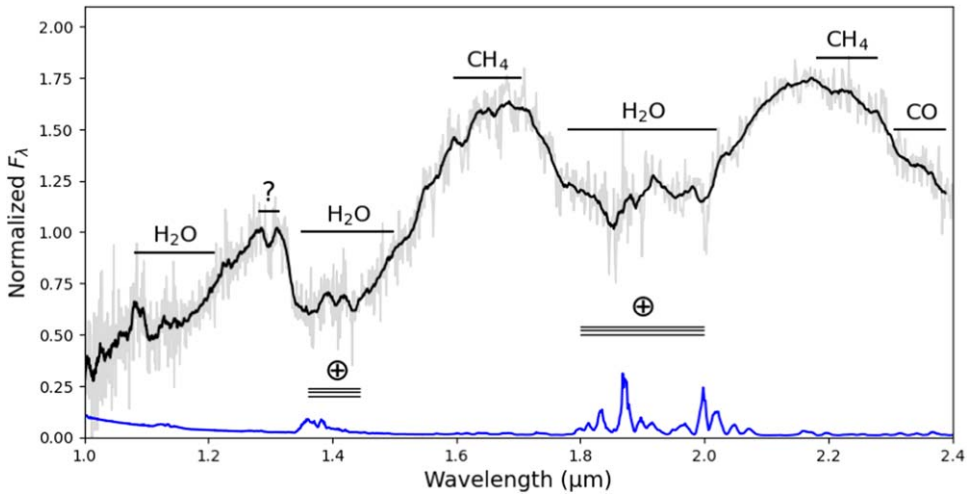

Figure 1. Magellan/FIRE spectrum of VHS J1831−5513 (black), Gaussian smoothed using a width of 15 pixels. Key molecular absorption features are labeled. Original resolution data are plotted in gray and flux uncertainty is shown in blue.
(The data used to create this figure are available in the online article.)

low-resolution prism mode using the 0.″8 slit (resolution $\lambda/\Delta\lambda \sim 100$) covering the full 0.8−2.5 μm wavelength range. The source was observed in an ABBA pattern with 16 individual exposures of 120 s each, using the Sample Up the Ramp (or SUTR) read mode. Immediately after the science image, we obtained a neon, neon, argon lamp and the A0 star HD 153842 for telluric, wavelength, and flux calibration. All data were reduced using a custom version of the `FIREHOSE` (Gagné et al. 2015b) package. The pipeline was modified such that boxcar extractions were performed on A-B images to avoid large variations in the slope of the resulting spectra, and subroutines from the SpeXtool v1 package (Vacca et al. 2003; Cushing et al. 2004) were used to combine, mask, and inspect the resulting spectra.

The final reduced spectrum is shown in Figure 1, in which prominent absorption features and telluric bands are labeled. We caution that due to the nonlinear response of the detector, the slope after the ∼2.3 μm CO edge may be unreliable as response decreases rapidly toward the edge of the detector.

4. Analysis

4.1. Spectral Type

The left panel of Figure 2 compares the near-infrared spectrum of VHS J1831−5513 to several field-age L/T transition spectral standards (Burgasser et al. 2006; Kirkpatrick et al. 2010; Cruz et al. 2018). The extremely red spectral slope and low-gravity features (e.g., steep *H*-band slope) in the near-infrared spectrum of VHS J1831−5513 leads to poor fits to the spectral standards over the 1–2.4 μm range as a whole, as is the case for many other young, red objects (e.g., Faherty et al. 2013; Liu et al. 2013; Schneider et al. 2016, 2023a). The best fit over the *J* band is the L9 standard 2MASS J02550357−4700509 (Kirkpatrick et al. 2010). Although progress is being made in the spectral classification of young L and T dwarfs (e.g., Piscarreta et al. 2024), there is not yet a unified approach tailored to young objects, nor a complete set of young L/T transition spectral standards. The diversity seen in the near-infrared slopes and molecular absorption features within the known young populations remains a challenge for the development of a uniform classification technique of young objects. The right panel of Figure 2 compares VHS J1831−5513 to the young, red objects WISEA J114724.10−204021.3 (WISEA J1147−2040; L7γ; Schneider et al. 2016), PSO J318.5338−22.8603 (PSO J318.5−22; L7 VL-G; Liu et al. 2013), and CWISE J050626.96+073842.4 (L8–T0γ; Schneider et al. 2023a). These comparisons highlight the extremely red near-infrared slope of VHS J1831−5513, which is noticeably redder than many members of the young planetary-mass population, and is matched only by CWISE J0506+0738, the reddest free-floating L/T dwarf currently known.

Like CWISE J0506+0738, the spectrum of VHS J1831−5513 displays likely CH_4 absorption features at the *H*-band peak and on the red side of the *K*-band peak. These features also occur in the spectrum of another young, planetary-mass L dwarf, VHS 1256−1257 b. The left column of Figure 3 compares the *H* and *K* bands of the Magellan/FIRE spectrum of VHS J1831−5513 and the JWST spectrum of VHS 1256−1257 b (Miles et al. 2023). The two objects have several likely CH_4 absorption features in common, as highlighted in the left column of Figure 3. The wavelengths of these features coincide with CH_4 absorption bands that begin to form in model spectra of low-gravity objects at effective temperatures $\lesssim$1500 K and become more prominent as the temperature decreases. The right column of Figure 3 shows Sonora Bobcat (Marley et al. 2021) models at solar metallicity and a constant surface gravity ($\log(g) = 3.5$), with temperatures ranging from 1100 K to 1500 K. Highlighted are the locations of the absorption features that occur in the spectra of both VHS J1831−5513 and VHS 1256−1257 b.

Unlike CWISE J0506+0738 and VHS 1256−1257 b, VHS J1831−5513 displays a prominent absorption feature at the peak of the *J* band, centered at ∼1.3 μm. This feature is not reproduced by the Sonora models and, to our knowledge, no feature centered at this wavelength has previously been noted in other L dwarfs. In T dwarfs, a 1.3 μm CH_4 band is responsible for the gradually increasing downward slope on the red side of the *J*-band peak, starting in early-T dwarfs and progressing through later subtypes. It eventually merges with

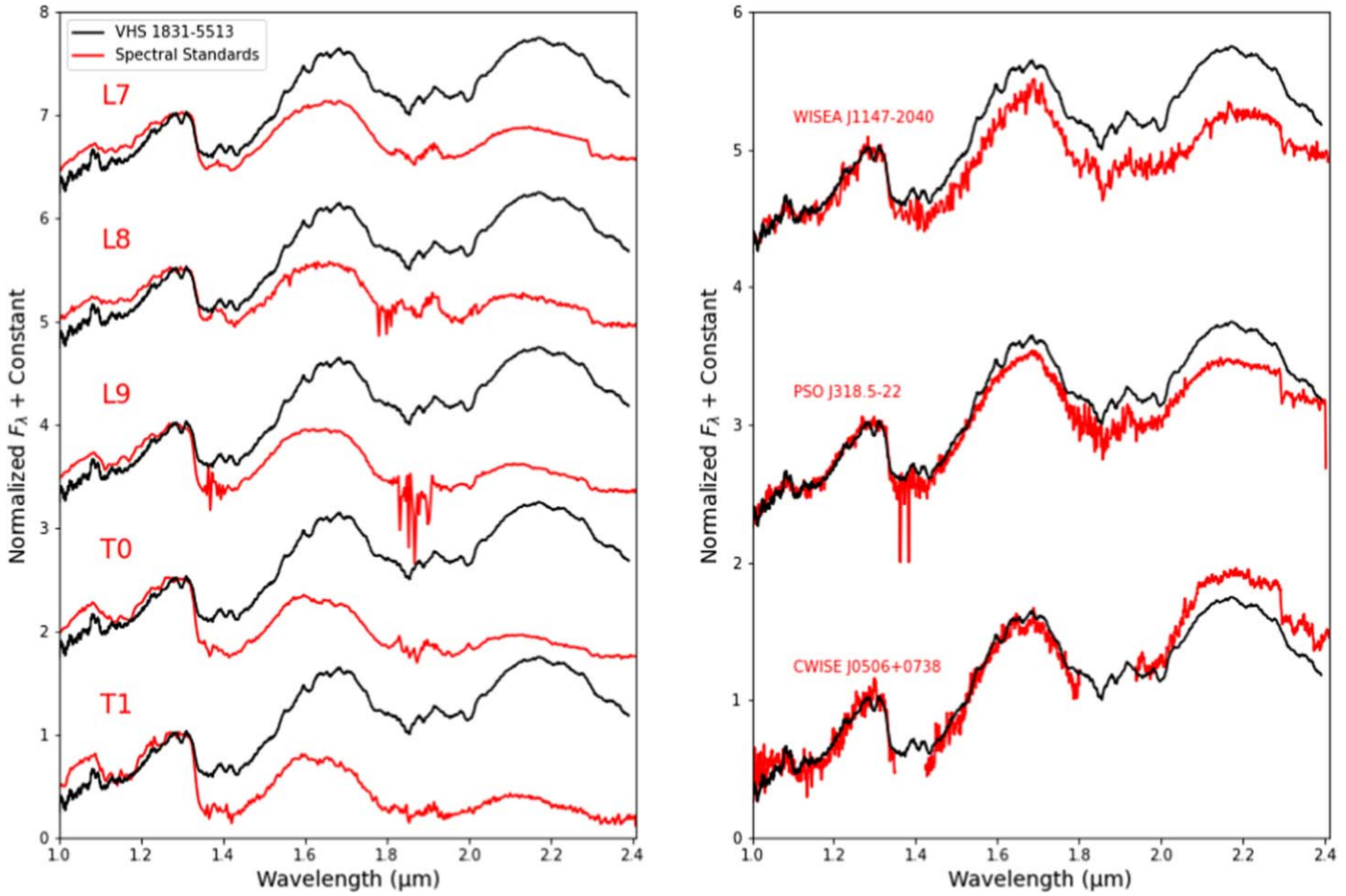

Figure 2. Left: smoothed Magellan/FIRE spectrum of VHS J1831−5513 (black) compared to the spectral standards (red, labeled) 2MASS J08251968+2115521 (L7) from Cruz et al. (2018), 2MASS J16322911+1904407 (L8) and 2MASS J02550357−4700509 (L9) from Kirkpatrick et al. (2010), and SDSS J120747.17+024424.8 (T0) and SDSS J083717.21−000018.0 (T1) from Burgasser et al. (2006). Right: VHS J1831−5513 compared to the young, planetary-mass objects WISEA J1147−2040 (Schneider et al. 2016), PSO J318.5−22 (Liu et al. 2013), and CWISE J0506+0738 (Schneider et al. 2023a). All spectra are normalized between 1.27 and 1.29 μm.

the 1.4 μm H_2O band to produce the characteristic, thin *J*-band peak of late-T dwarfs (Burgasser et al. 2002). Given the presence of likely CH_4 absorption elsewhere in the spectrum of VHS J1831−5513, the observed 1.3 μm feature may also be the result of CH_4 absorption. Given that such absorption has only been seen in T dwarfs, this would be suggestive of VHS J1831−5513 being narrowly on the T side of the L/T transition. However, we caution that CH_4 is not known to exhibit any sharp features in this area, and this would therefore be a very unusual presentation for CH_4 absorption. There is a known telluric O_2 feature close to the wavelength in question (though not at the exact wavelength) which may cause contamination (Kausch et al. 2015, and references therein). We therefore inspected the raw science and telluric data to check if the feature was the result of poor telluric correction, but no obvious cause was found. The feature also does not appear in any of the other spectra taken with the instrument on the night. For now, we are uncertain of the feature's cause, and characterize it as an unknown absorber. Future acquisition of higher-resolution, higher-signal-to-noise ratio (S/N) spectra will allow this feature to be investigated further using the spectral inversion (retrieval) technique, which has been effectively utilized in recent studies to constrain cloud properties and elemental abundances of substellar objects (e.g., Burningham et al. 2021; Calamari et al. 2022; Adams et al. 2023; Hood et al. 2023; Vos et al. 2023; Whiteford et al. 2023).

Considering the L9 standard being the best *J*-band fit, the deep 1.1 μm H_2O band, and the *H*- and *K*-band CH_4 absorption features, we assigned a preliminary spectral type of L8–T0 (very red), prior to gravity assessment.

4.2. Gravity

Although the extremely red near-infrared colors of VHS J1831−5513 are a potential indicator of youth, a small population of field-gravity objects are also known to possess red colors (e.g., Marocco et al. 2014), possibly due to an excess of sub-micron-sized dust grains in their photospheres (Hiranaka et al. 2016). A near equator-on inclination angle has also been found to be a cause of red colors among field objects (Vos et al. 2017; Guerra Toro et al. 2022; Suárez et al. 2023), indicating that red colors in brown dwarfs are more complex diagnostically than previously thought. Hence, other spectral diagnostics must be performed to confirm youth.

Youth in brown dwarfs and planetary-mass objects can also be inferred through evidence of low surface gravity, as young objects are still contracting (Burrows et al. 1997) and have larger radii than equivalent-temperature field objects. Intermediate- and low-surface-gravity objects, suffixed β and γ,

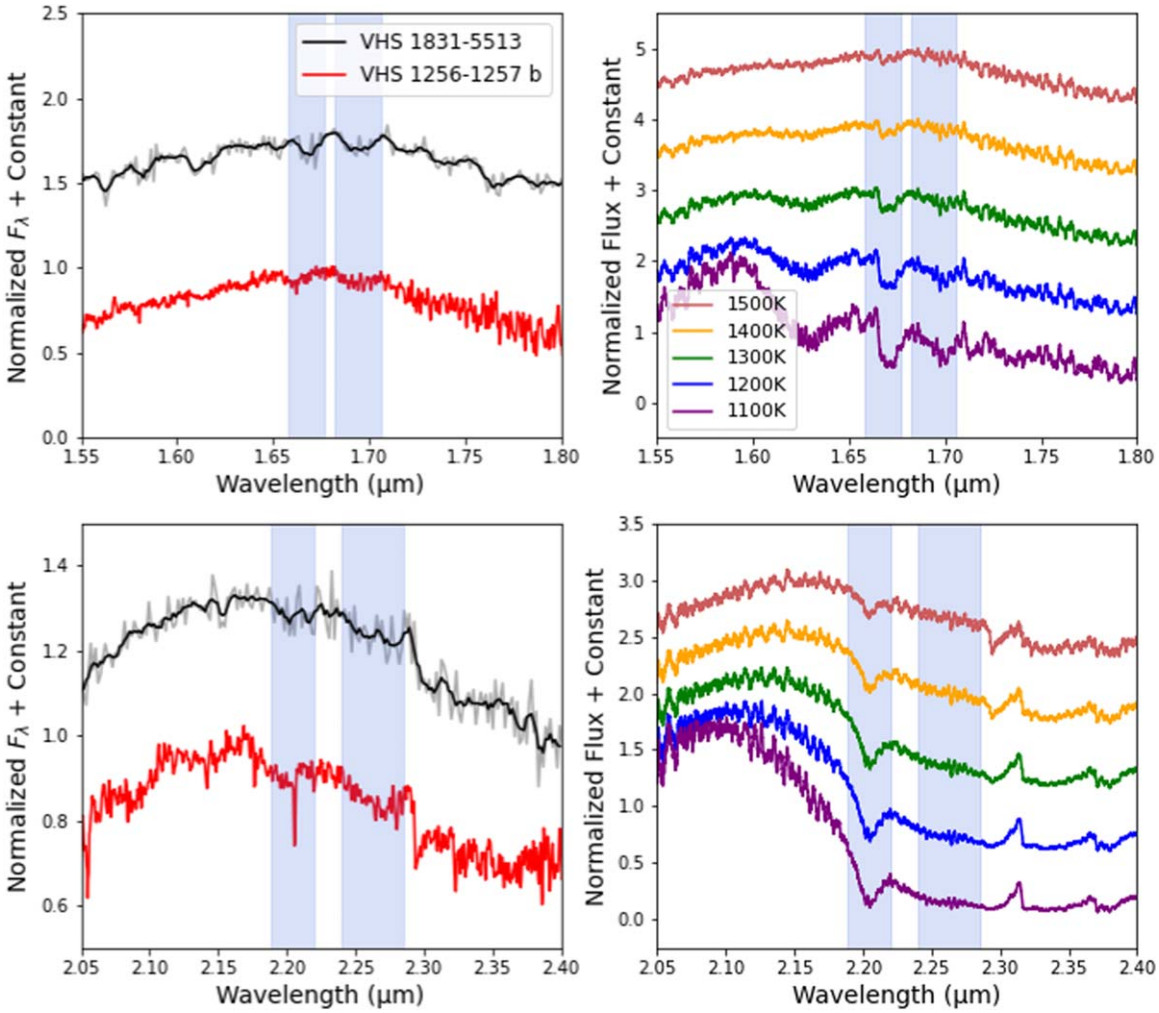

Figure 3. Left: comparison between the *H* (top) and *K* (bottom) bands of VHS J1831−5513 (black, smoothed; gray, original resolution) and the young, planetary-mass companion VHS 1256–1257 b (red; Miles et al. 2023). CH_4 absorption features that appear in both objects are marked by blue bands. Right: Sonora Bobcat (Marley et al. 2021) models at solar metallicity and $\log(g) = 3.5$, with a range of effective temperatures. The blue bands represent the locations of the absorption features in the corresponding band of the left column.

respectively (Kirkpatrick 2005; or INT-G and VL-G as per Allers & Liu 2013 indices), can be discerned from field-gravity objects by utilizing morphological differences in their optical and near-infrared spectra. Gravity-sensitive indices are well established for early-to-mid-type L dwarfs (Lucas et al. 2001; McGovern et al. 2004; Kirkpatrick et al. 2006; Cruz et al. 2009, 2018; Allers & Liu 2013; Martin et al. 2017). Some rely on the weakening of atomic lines in the spectra of lower-gravity objects. Others measure the shape of spectral regions, the morphologies of which are particularly affected by the strength of H_2 CIA, which is reduced in lower-gravity objects. However, most gravity-sensitive indices do not function well for late-type L dwarfs (>L5).

One index that may function for objects as late in type as VHS J1831−5513 is the *H*-slope index (Schneider et al. 2023a). Low-gravity (young) objects have more peaked *H* bands caused by reduced H_2 CIA in their low-pressure photospheres. The *H*-slope index aims to quantify this by using a linear least-squares fit between 1.45–1.64 μm to measure the slope of the blue side of the *H* band, where the unit is normalized flux/wavelength. Schneider et al. (2023a) found that for L7–T0 dwarfs, typical field-gravity objects have *H*-slope values ranging from 2 to 4, and low-gravity objects have values between 3 and 5. VHS J1831−5513 has an *H*-slope value of 5.068, considerably higher than those of field objects, and even slightly exceeding the top end of the young population. This result is extremely similar to that of the spectrum of CWISE J0506+0738, which returns an *H*-slope value of 5.043.[14]

The $H_2(K)$ index (Canty et al. 2013) has also been shown to differentiate low-gravity and field-gravity objects at late-L subtypes (Schneider et al. 2014). Like the *H*-cont and *H*-slope indices, it utilizes the reduced H_2 CIA that occurs in lower-gravity objects, but in the *K* band. To do this, it measures the slope between 2.17 and 2.24 μm by calculating the ratio of the median fluxes in 0.02 μm ranges centered at those wavelengths in the unsmoothed spectrum of an object. For L7–T0 spectral types, typical index scores for field-gravity objects are $1.05 \leqslant H_2(K) \leqslant 1.2$, whereas low-gravity objects score much lower than their field-gravity counterparts of the same spectral type (Schneider et al. 2014). VHS J1831−5513 returns a score of $H_2(K) = 1.045$, over 1σ below the field sequence at L7, and

[14] Schneider et al. (2023a) reported an *H*-slope value of 4.38 for CWISE J0506+0738, calculated before rescaling to correct for Keck/NIRES inter-band flux-calibration issues. Our value for CWISE J0506+0738 is calculated using its spectrum rescaled to its photometric $J - K$ color.

Table 2
BANYAN Σ Membership Results

Input Data	Group Membership Probability[a] (%)	d_{opt}[b] (pc)
μ	BPMG (79.7), ARG (8.6), ABDMG (2), Field (9.8)	BPMG (51.5 ± 5.1), ARG (54.8 ± 5.8), ABDMG (67.1 ± 6)
$\mu + d_{phot}$	BPMG (85.2), ARG (9.7), ABDMG (0.4), Field (4.6)	–

Notes.
[a] ABDMG = AB Doradus Moving Group (Zuckerman et al. 2004); ARG = Argus Association (Torres et al. 2008); BPMG = β Pictoris Moving Group (Zuckerman et al. 2001); Field = Not a member of any known group.
[b] Optimal distance to VHS J1831−5513, assuming membership of individual groups.

significantly further below for later spectral types (∼3σ below for L8), where the field sequence sees a rapid increase (see Figure 10 of Schneider et al. 2014).

We caution that as most of these indices predate the discovery that inclination angle is correlated with cloud opacity (Vos et al. 2017; Guerra Toro et al. 2022; Suárez et al. 2023), they are not designed to account for this and, as such, it is possible that the viewing geometry of VHS J1831−5513 may interfere with the gravity assessment they provide. The existence of such contamination and extent to which this may impact the index scores is yet to be fully tested.

Considering the extremely red near-infrared slope, the *H*-slope and $H_2(K)$ indicators, and the probable kinematic match to the ∼22 Myr BPMG (Zuckerman et al. 2001; Shkolnik et al. 2017) discussed later, we conclude that VHS J1831−5513 has low surface gravity, and tentatively classify it as L8γ–T0γ. Both a higher-S/N spectrum and the future development of gravity-sensitive indices applicable to L/T transition objects will contribute to a higher-confidence gravity assessment for VHS J1831−5513.

5. Discussion

5.1. Moving Group Membership

Young moving groups typically retain similar 3D velocities for a few hundred million years, and their population encompasses the whole range of masses from planetary mass to stars (Zuckerman & Song 2004; Torres et al. 2008; Malo et al. 2013; Gagné et al. 2014; Faherty et al. 2016). Young moving groups are coeval, so objects that are found to be a member of a group can be assigned the age of that group and become key benchmarks for its population.

To determine if VHS J1831−5513 is a member of a known young moving group, we used the BANYAN Σ algorithm (Gagné et al. 2018c), which uses Bayes' theorem to select the best-matching XYZUVW model among 27 young associations and the distribution of nearby field stars, while optionally marginalizing over missing radial velocities or distances with an exact, analytical solution to the marginalization integrals. BANYAN Σ requires minimum inputs of position and proper motions, and can optionally use distance and heliocentric radial velocity with respective uncertainties. If distance and/or radial velocity are not provided, it calculates and provides optimal values for these, assuming membership in each of the 27 groups.

The long time baseline of CatWISE (12 epochs over 8 yr) means that it can provide proper-motion measurements with reasonable confidence (± ∼10 mas yr^{-1} for a W1 = 14 mag source; Marocco et al. 2021). We therefore use the CatWISE proper-motion data for the BANYAN Σ input. However, CatWISE has known systematic astrometric offsets compared to Gaia Data Release 2.[15] We therefore applied the offsets for the CatWISE tile in which VHS J1831−5513 is located, and used the corrected proper-motion values for our BANYAN Σ input. When only provided with the position and proper motions of VHS J1831−5513, with respective uncertainties, BANYAN Σ gives a 79.7% membership probability for the ∼22 Myr BPMG (Zuckerman et al. 2001; Shkolnik et al. 2017), an 8.6% probability for the ∼45 Myr Argus Association (ARG; Torres et al. 2008; Zuckerman 2019), a 2% probability for the ∼130 Myr AB Doradus moving group (ABDMG; Zuckerman et al. 2004; Gagné et al. 2018b), and a 9.8% probability of VHS J1831−5513 not being a member of any known group.

VHS J1831−5513 is too faint at optical wavelengths to be detected by the Gaia mission (Gaia Collaboration et al. 2023), and in surveys where it *is* detected, insufficient astrometric data of adequate precision to determine a parallax exist. We instead calculated a photometric distance for VHS J1831−5513. As has been noted in previous works, objects with unusual near-infrared colors do not conform well to standard absolute magnitude relations (Faherty et al. 2013; Filippazzo et al. 2015; Faherty et al. 2016; Liu et al. 2016). In investigating this, Schneider et al. (2023a) compared the parallactic distances of several very red, free-floating objects to their *J*, *K*, W1, and W2 photometric distances, and showed that for those objects, the *K*-band photometric distance provided the best match on average to the measured parallax. We therefore used the VHS K_s-band magnitude to calculate a photometric distance for VHS J1831−5513 using the absolute magnitude–spectral type relations in Dupuy & Liu (2012). Using a spectral type of L9 ± 1, we determine a K_s-band photometric distance for VHS J1831−5513 of 55.4 ± 5.5 pc. This distance agrees well with the optimal kinematic distances for BPMG (51.5 ± 5.1 pc) and ARG (54.8 ± 5.8 pc) membership provided by BANYAN Σ. Adding this photometric distance to the existing position and proper-motion parameters, BANYAN Σ gives an 85.2% membership probablity for BPMG, 9.7% for ARG, 0.4% for ABDMG, and 4.6% for no group. While promising, this is not a conclusive indicator of BPMG membership, as a probability of >90% is typically used as a cutoff to select high-probability group members (Gagné et al. 2015a). Regardless, the indications of low surface gravity in its spectrum and the fairly low-precision proper-motion measurements from CatWISE for VHS J1831−5513 merit further investigation of a ∼85% membership probability. A summary of the BANYAN Σ results are provided in Table 2.

[15] https://irsa.ipac.caltech.edu/data/WISE/CatWISE/gator_docs/CatWISE2020_Table1_20201012.tbl

In light of its positive spectral indicators of youth and its best BANYAN Σ kinematic match, we find that VHS J1831−5513 is most likely a member of the BPMG. A higher-precision proper-motion measurement as well as future radial velocity and trigonometric parallax measurements are required to confirm or refute this membership.

5.2. Physical Properties

Under the assumption that it is a member of the BPMG, certain physical properties of VHS J1831−5513 can be inferred. Viana Almeida et al. (2009) found that the BPMG has approximately solar metallicity, so we assume solar metallicity for our analysis. First, we estimated the bolometric luminosity of VHS J1831−5513. To do this, we used the Sanghi et al. (2023) empirical bolometric correction–spectral type polynomial relations for young objects, in combination with the absolute VHS K_s-band magnitude based on our previously calculated photometric distance. We estimate a bolometric luminosity for VHS J1831−5513 of $\log(L_{\rm bol}/L_\odot) = -4.57 \pm 0.09$. Note that several assumptions are made when determining this value, such as our photometric distance being accurate and the Sanghi et al. (2023) relations being applicable to such an unusually red object. A more accurate bolometric luminosity can be determined with a measured parallax and broader wavelength coverage.

To test this value, we also derive a bolometric correction for VHS 1256–1257 b using the bolometric luminosity from Miles et al. (2023) and photometry from the Ultracoolsheet (Best et al. 2024, and references therein), and apply it to VHS J1831−5513. VHS 1256–1257 b is known to be red and young, and the broad wavelength coverage provided by the JWST observations of this object allows for a precise determination of its $L_{\rm bol}$ value. This yields a value of $\log(L_{\rm bol}/L_\odot) = -4.51 \pm 0.09$ for VHS J1831−5513.

We used the Sonora Bobcat (Marley et al. 2021) and Diamondback (Morley et al. 2024) evolutionary models at solar metallicity to estimate the mass and radius of VHS J1831−5513 using the age of the BPMG (22 ± 6 Myr; Shkolnik et al. 2017) and the bolometric luminosity derived from the Sanghi et al. (2023) relations. Using the Sonora Bobcat models, assuming BPMG membership, we infer a radius of $1.32^{+0.03}_{-0.02}$ $R_{\rm Jup}$ and a mass of 7 ± 1 $M_{\rm Jup}$. Using the calculated bolometric luminosity, derived radius, and the Stefan–Boltzmann law, we estimate an effective temperature for VHS J1831−5513 of $T_{\rm eff} = 1130 \pm 60$ K. From the Sonora Diamondback models, taking the same age and bolometric luminosity, we infer a radius of $1.42^{+0.04}_{-0.03}$ $R_{\rm Jup}$, a mass of 6.5 ± 1.5 $M_{\rm Jup}$, and an effective temperature of $T_{\rm eff} = 1085 \pm 60$ K.

While both models suggest a similar mass and effective temperature for VHS J1831−5513, the radius is notably different. The Diamondback values are preferred, as the model incorporates silicate clouds, as well as gravity-dependent cloud clearing, which appears to occur at the L/T transition (Marley et al. 2010). In both cases, the mass is well below the deuterium burning limit of ∼13 $M_{\rm Jup}$ (Spiegel et al. 2011, and references therein) and the effective temperature is ∼150-200 K cooler than an L9 at field age (Kirkpatrick et al. 2021), which is consistent with previous findings that young objects are cooler than field-age objects of equivalent spectral type (Filippazzo et al. 2015; Faherty et al. 2016; Liu et al. 2016; Suárez et al. 2021). An insufficient number of L/T transition objects are currently known in BPMG to infer the temperature at which the L/T transition occurs in the group. However, the temperature at which the L/T transition occurs decreases with age, and Gagné et al. (2018a) found that the L/T transition for ABDMG is ∼1150 K, suggesting that if VHS J1831−5513 is a true member of BPMG, the L/T transition may occur at a similar temperature in the two groups, despite the ∼100 Myr age difference.

VHS J1831−5513 is notably ∼100 K cooler than PSO J318.5−22 (Miles et al. 2018), which displays no corresponding near-infrared CH_4 absorption features. It is, however, an extremely similar effective temperature to CWISE J0506+0738 ($T_{\rm eff} = 1140 \pm 80$ K; Schneider et al. 2023a), which exhibits likely CH_4 absorption at both the *H*- and *K*-band peaks. This temperature similarly bolsters the empirical temperature constraint provided by CWISE J0506+0738 for the introduction of CH_4 absorption into the near-infrared spectra of young L/T transition objects.

BANYAN Σ returns a nonzero probability of VHS J1831−5513 being a member of ABDMG, which has very similar *UVW* and distance values among its membership to that of BPMG. These similarities are known to confuse membership assignment for some objects between the two groups (Gagné et al. 2018c). In case of the unlikely event that VHS J1831−5513 is an ABDMG member, we repeated the analysis using the age of the ABDMG (133^{+15}_{-20} Myr; Gagné et al. 2018b). Assuming ABDMG membership, the Marley et al. (2021) models suggest a radius of $1.23^{+0.13}_{-0.11}$ $R_{\rm Jup}$, an effective temperature of 1170 ± 50 K, and a mass of 12 ± 0.2 $M_{\rm Jup}$ for VHS J1831−5513. This would still place VHS J1831−5513 below the deuterium burning limit, solidifying its status as a planetary-mass object. We reiterate that the scenario where VHS J1831−5513 is a member of ABDMG is unlikely, and BPMG is the strong favorite for membership.

5.3. Prospects for Variability

Young L and T dwarfs are known to exhibit stronger photometric and spectrophotometric variability than field-age objects, driven by rotational modulations of condensate clouds in their atmospheres (Biller et al. 2015; Metchev et al. 2015; Lew et al. 2016; Biller et al. 2018; Schneider et al. 2018; Vos et al. 2018; Eriksson et al. 2019; Miles-Páez et al. 2019; Vos et al. 2019; Bowler et al. 2020; Vos et al. 2020; Manjavacas et al. 2021; Vos et al. 2022). Furthermore, the L/T transition has been shown to have a higher-variability occurrence rate than other spectral types (Radigan 2014). Indeed, Liu et al. (2024) determined that the variability rate of young objects at the L/T transition is 64^{+23}_{-22}%, compared to 31^{+12}_{-9}% outside the L/T transition. Variable L dwarfs are more likely to have cloudier atmospheres (Suárez & Metchev 2022) and redder colors (Ashraf et al. 2022) than nonvariable counterparts. Additionally, both variability amplitude and infrared colors have been found to be correlated with inclination angle, with equator-on objects having higher amplitudes and redder colors than those which are viewed pole-on (Vos et al. 2017). Near-infrared colors also depend on cloud thickness, where redder L dwarfs have higher cloud opacity than bluer objects (Suárez & Metchev 2022).

Suárez et al. (2023) further demonstrated a correlation between infrared color, cloud opacity, and viewing inclination for L dwarfs, finding that equator-on objects exhibit more clouds and therefore are redder than objects viewed close to pole-on. This indicates that equatorial latitudes are cloudier

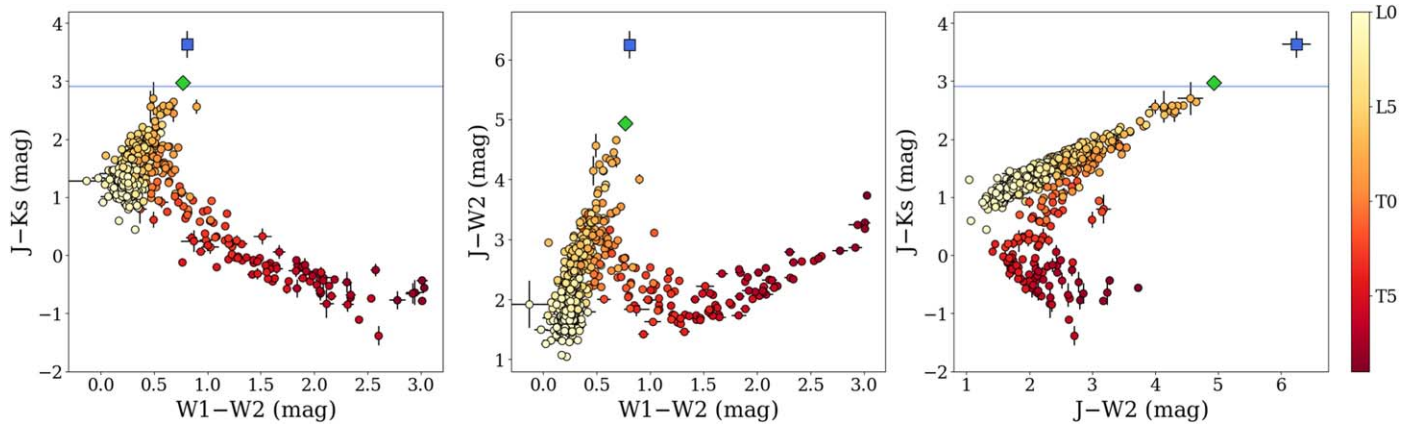

Figure 4. Color–color diagrams comparing VHS J1831−5513 (blue square) to L and T dwarfs with photometry from Schneider et al. (2023b; yellow to red circles) and CWISE J0506+0738 (green diamond; Schneider et al. 2023a). VHS J1831−5513 is plotted using its VHS and CatWISE photometry, and represents a significant outlier from even the reddest known objects. The blue lines in the left and right plots indicate the synthetic $J - K_S$ color calculated from the Magellan/FIRE spectrum of VHS J1831−5513, which is still an outlier from the bulk of the brown dwarf population, but is similar to that of CWISE J0506+0738, the reddest known L/T transition dwarf.

than polar latitudes and the color diversity of brown dwarfs is strongly influenced by their viewing geometry.

The VHS photometry of VHS J1831−5513 indicates a color of $J - K_S = 3.633 \pm 0.277$ mag. However, visual inspection and comparison of its Magellan/FIRE spectrum showed that its spectrum is not as red as CWISE J0506+0738 (see Figure 2), which has a color of $(J - K)_{MKO} = 2.974 \pm 0.039$ mag (Schneider et al. 2023a). We therefore extracted synthetic photometry from the spectrum of VHS J1831−5513 using a custom code with filter profiles from Spanish Virtual Observatory's Filter Profile Service (Rodrigo et al. 2012; Rodrigo & Solano 2020). This gives a color of $(J - K_S)_{synth} = 2.914 \pm 0.008$ mag, which is discrepant from the VHS color by 0.719 mag (3.07σ). The photometric and synthetic colors of VHS J1831−5513 are compared to the photometric colors of CWISE J0506+0738 and other L and T dwarfs in Figure 4.

The VHS J- and K_s-band exposures were taken ∼6 minutes apart, so can be treated as near simultaneous; the shortest known variability period of a brown dwarf is ∼1.08 hr (Tannock et al. 2021; Vos et al. 2022), and young brown dwarfs are known to be slow rotators (Schneider et al. 2018; Vos et al. 2022). Thus, such a short time difference should be insufficient to cause a significant enough photometric change to explain the observed color discrepancy in VHS J1831−5513.

While we cannot definitively rule out that the sole cause of the color discrepancy is the low S/N of the VHS J-band detection (S/N ≈ 4.6), we note that VHS J1831−5513 possesses exceptionally red near-infrared colors, which is suggestive of an extreme atmosphere, potentially viewed near equator-on. Complex clouds, disequilibrium chemistry, and powerful atmospheric dynamics may be expected in such a young, red atmosphere (Showman & Kaspi 2013; Suárez & Metchev 2023; Suárez et al. 2023), and can affect the emergent flux observed from the object. It is therefore possible that cloud-driven variability in VHS J1831−5513 may contribute to the observed $(J - K_S)$ color discrepancy. The ∼9 yr difference between the VHS images being taken and the Magellan/FIRE spectrum being collected is easily sufficient for variability to have played a role in causing the discrepancy between the two.

Pressure plays a key role in the behavior of clouds within the atmospheres of substellar objects (Buenzli et al. 2012; Yang et al. 2016). With the J and K_S bands probing different atmospheric depths, they may exhibit different variability amplitudes, as has been observed in other L/T transition objects, which show higher amplitudes in the J band than the K_S band (Artigau et al. 2009; Radigan et al. 2012; Vos et al. 2019). VHS 1256−1257 b, an object similar in nature to VHS J1831−5513, is highly variable in the J band, with both Bowler et al. (2020) and Zhou et al. (2020) finding a 1.27 μm variability amplitude of ∼25 %, and Zhou et al. (2022) finding a broader J-band variation of up to 38% on a ∼1 yr timescale, the highest ever observed in a substellar object. In the same vein, phase shifts between J and K_S light curves can also affect the $J - K_S$ color of L/T transition dwarfs (e.g., McCarthy et al. 2024; Plummer et al. 2024). Future time-resolved monitoring will provide insight into whether differing variability amplitudes and/or a phase shift between the J and K_S bands of VHS J1831−5513 exist, and, if so, to what extent they impact its $J - K_S$ color.

The correlation between near-infrared color, viewing inclination, and cloud opacity in Suárez et al. (2023) is helpful to understand the appearance of objects like VHS J1831−5513. This may indicate that its extremely red near-infrared colors and potentially the CH_4 features in its Magellan/FIRE spectrum are explained, at least partially, by unusually thick clouds as a consequence of the object being viewed equator-on. We note, however, that the Suárez et al. (2023) study focused on L3–L7 dwarfs and did not take into account objects as late in type as VHS J1831−5513. L7 marks the peak for $J - K$ colors on the field sequence as objects at later types rapidly get bluer as condensates sink below the photosphere. While the trends between near-infrared color and inclination in Vos et al. (2017) and Vos et al. (2020) are observed into the L/T transition, it is an evolutionary stage in which marked changes, both chemical and physical, occur in the atmospheres of brown dwarfs, so further investigation is needed to determine if the trends identified in Suárez et al. (2023) are applicable to the L/T transition.

The only multi-epoch survey to detect VHS J1831−5513 is the WISE mission. However, because of the latent artifact contamination described in Section 2, we were unable to confidently explore the variability properties of VHS J1831−5513 using the WISE data. Nonetheless, VHS 1831−5513 is highly likely to exhibit detectable variability given its red

infrared colors, young age, possible near equator-on inclination angle and cloudy atmosphere, and its position at the L/T transition (Radigan 2014; Vos et al. 2017, 2019; Suárez & Metchev 2022), making it a promising target for future variability studies.

6. Conclusion

We have presented the discovery of VHS J1831−5513, an extremely red, young L/T transition object, identified through a search of the CatWISE reject and VHS catalogs. We obtained Magellan/FIRE near-infrared spectroscopy of VHS J1831−5513, which shows that it is an ∼L8γ–T0γ dwarf with likely CH_4 absorption at the *H*- and *K*-band peaks. The presence of CH_4 in the atmosphere of VHS J1831−5513 indicates a $T_{\rm eff}$ at the L/T transition. We find that its spectral morphology is similar to those of other young, red, late-type L dwarfs, including the planetary-mass companion VHS 1256−1257 b, with which it shares a number of individual CH_4 absorption features. VHS J1831−5513 also exhibits a 1.3 μm absorption feature, the cause of which is unclear. This feature must be investigated further, potentially at higher resolution, in order to confidently assert its cause.

Using the BANYAN Σ Bayesian algorithm, we determine that VHS J1831−5513 is a likely member of the ∼22 Myr BPMG based on its kinematics. This membership assignment is supported by its low-gravity score in pressure-sensitive indices and its red near-infrared slope. Future trigonometric parallax, radial velocity, and higher-precision proper-motion measurements will help to test this membership. Using the age of BPMG, we inferred physical properties for VHS J1831−5513. Its estimated mass of 6.5 ± 1.5 $M_{\rm Jup}$ places it among the lowest-mass free-floating BPMG members known (alongside CWISE J0506+0738 at 7 ± 2 $M_{\rm Jup}$; Schneider et al. 2023a), contributing to empirical constraints on the group's initial mass function. Its estimated effective temperature of $T_{\rm eff} = 1085 \pm 60$ K is well below that of field-age objects of similar spectral types, consistent with previous findings for other young brown dwarfs. Given the spectroscopic evidence of the presence of CH_4 in its atmosphere, this temperature estimate also places empirical constraints on the temperature at which CH_4 begins to appear in the near-infrared spectra of young L/T transition dwarfs.

The extremely red near-infrared colors and potentially near equator-on inclination angle of VHS J1831−5513 make it highly likely to be extremely cloudy. This, in combination with its young age and position at the L/T transition, suggests that VHS J1831−5513 is highly likely to be variable, and is therefore an excellent prospective target for future photometric and spectrophotometric monitoring. A significant ($\sim 3.1\sigma$) $J - K_S$ color discrepancy noticed between its Magellan/FIRE spectrum and VHS photometry may also indicate that it has a significant difference between its *J*- and K_s-band variability amplitudes or a potential phase shift between its *J*- and K_S light curves, making it a yet more intriguing target for variability monitoring.

The discoveries of VHS J1831−5513 in this work and CWISE J0506+0738 in Schneider et al. (2023a) hint at the existence of a population of exceptionally red L/T transition objects, which until the introductions of newer near-infrared surveys with deeper detection thresholds were simply too faint to be detected in the *J* band by the previous generation of near-infrared survey instruments (e.g., 2MASS). Future targeted searches of these catalogs are warranted to discover more examples of such extraordinarily red objects. This also highlights the importance of the upcoming Euclid mission (Laureijs et al. 2011), which has an expected 5σ point source *J*-band depth of ∼24.5 mag (Euclid Collaboration et al. 2022), and so will be able to detect not only intrinsically fainter red objects but red objects at further distances, expanding the census of known red objects and enabling a better understanding of their space density, a key component for exploring the mass functions of nearby associations.

VHS J1831−5513 is an excellent prospective JWST target to facilitate atmospheric retrieval studies with high-resolution data. This would also represent an excellent opportunity to probe the L/T transition at young ages—an area not yet fully understood, primarily due to the paucity of known young L/T transition objects.

Acknowledgments

The Backyard Worlds: Planet 9 team would like to thank the many Zooniverse volunteers who have participated in this project. We would also like to thank the Zooniverse web development team for their work creating and maintaining the Zooniverse platform and the Project Builder tools. This research was supported by NASA grant No. 2017-ADAP17-0067. This material is supported by the National Science Foundation under grant Nos. 2007068, 2009136, and 2009177. J.F. acknowledges the Heising Simons Foundation as well as NSF award #1909776, and NASA Award #80NSSC22K0142. J.M.V. acknowledges support from a Royal Society - Science Foundation Ireland University Research Fellowship (URF\1\221932). This research made use of the Montreal Open Clusters and Associations (MOCA) database, operated at the Montréal Planétarium (J. Gagné et al., in preparation). This paper includes data gathered with the 6.5 m Magellan Telescopes located at Las Campanas Observatory, Chile. This publication makes use of data products from the Wide-field Infrared Survey Explorer, which is a joint project of the University of California, Los Angeles, and the Jet Propulsion Laboratory/California Institute of Technology, funded by the National Aeronautics and Space Administration. CatWISE was funded by NASA under Proposal No. 16-ADAP16-0077 issued through the Astrophysics Data Analysis Program, and uses data from the NASA-funded WISE and NEOWISE projects. This work uses data obtained as part of the VISTA Hemisphere Survey, ESO Progam, 179.A-2010 (PI: McMahon). This research has made use of the Spanish Virtual Observatory (https://svo.cab.inta-csic.es) project funded by MCIN/AEI/10.13039/501100011033/ through grant No. PID2020-112949GB-I00. This work has benefited from The UltracoolSheet at http://bit.ly/UltracoolSheet, maintained by Will Best, Trent Dupuy, Michael Liu, Aniket Sanghi, Rob Siverd, and Zhoujian Zhang.

Facilities: Magellan/FIRE, Paranal/VISTA, WISE

Software: `FIREHOSE` (Gagné et al. 2015b), SpeXtool v1 (Cushing et al. 2004), unTimely Catalog Explorer (Kiwy 2022), WiseView (Caselden et al. 2018)

ORCID iDs

Thomas P. Bickle https://orcid.org/0000-0003-2235-761X
Adam C. Schneider https://orcid.org/0000-0002-6294-5937
Jonathan Gagné https://orcid.org/0000-0002-2592-9612
Jacqueline K. Faherty https://orcid.org/0000-0001-6251-0573
Austin Rothermich https://orcid.org/0000-0003-4083-9962

Johanna M. Vos https://orcid.org/0000-0003-0489-1528
Genaro Suárez https://orcid.org/0000-0002-2011-4924
J. Davy Kirkpatrick https://orcid.org/0000-0003-4269-260X
Aaron M. Meisner https://orcid.org/0000-0002-1125-7384
Marc J. Kuchner https://orcid.org/0000-0002-2387-5489
Adam J. Burgasser https://orcid.org/0000-0002-6523-9536
Federico Marocco https://orcid.org/0000-0001-7519-1700
Sarah L. Casewell https://orcid.org/0000-0003-2478-0120
Dan Caselden https://orcid.org/0000-0001-7896-5791
Daniella C. Bardalez Gagliuffi https://orcid.org/0000-0001-8170-7072

References

Adams, A. D., Meyer, M. R., Howe, A. R., et al. 2023, AJ, 166, 192
Allers, K. N., & Liu, M. C. 2013, ApJ, 772, 79
Ashraf, A., Bardalez Gagliuffi, D. C., Manjavacas, E., et al. 2022, ApJ, 934, 178
Artigau, É., Bouchard, S., Doyon, R., & Lafrenière, D. 2009, ApJ, 701, 1534
Bell, C. P. M., Mamajek, E. E., & Naylor, T. 2015, MNRAS, 454, 593
Best, W. M. J., Dupuy, T. J., Liu, M. C., et al. 2024, The UltracoolSheet: Photometry, Astrometry, Spectroscopy, and Multiplicity for 4000+ Ultracool Dwarfs and Imaged Exoplanets, v2.0.0, Zenodo, doi:10.5281/zenodo.10573247
Biller, B. A., Vos, J., Bonavita, M., et al. 2015, ApJL, 813, L23
Biller, B. A., Vos, J., Buenzli, E., et al. 2018, AJ, 155, 95
Borysow, A., Jorgensen, U. G., & Zheng, C. 1997, A&A, 324, 185
Bowler, B. P., Zhou, Y., Morley, C. V., et al. 2020, ApJL, 893, L30
Buenzli, E., Apai, D., Morley, C. V., et al. 2012, ApJL, 760, L31
Burgasser, A. J., Geballe, T. R., Leggett, S. K., Kirkpatrick, J. D., & Golimowski, D. A. 2006, ApJ, 637, 1067
Burgasser, A. J., Kirkpatrick, J. D., Brown, M. E., et al. 2002, ApJ, 564, 421
Burningham, B., Faherty, J. K., Gonzales, E. C., et al. 2021, MNRAS, 506, 1944
Burrows, A., Marley, M., Hubbard, W. B., et al. 1997, ApJ, 491, 856
Calamari, E., Faherty, J. K., Burningham, B., et al. 2022, ApJ, 940, 164
Canty, J. I., Lucas, P. W., Roche, P. F., & Pinfield, D. J. 2013, MNRAS, 435, 2650
Caselden, D., Westin, P. I., Meisner, A., Kuchner, M., & Colin, G. 2018, WiseView: Visualizing motion and variability of faint WISE sources, Astrophysics Source Code Library, ascl:1806.004
Chauvin, G., Lagrange, A. M., Dumas, C., et al. 2004, A&A, 425, L29
Cruz, K. L., Kirkpatrick, J. D., & Burgasser, A. J. 2009, AJ, 137, 3345
Cruz, K. L., Núñez, A., Burgasser, A. J., et al. 2018, AJ, 155, 34
Cushing, M. C., Marley, M. S., Saumon, D., et al. 2008, ApJ, 678, 1372
Cushing, M. C., Vacca, W. D., & Rayner, J. T. 2004, PASP, 116, 362
Dupuy, T. J., & Liu, M. C. 2012, ApJS, 201, 19
Dye, S., Lawrence, A., Read, M. A., et al. 2018, MNRAS, 473, 5113
Eisenhardt, P. R. M., Marocco, F., Fowler, J. W., et al. 2020, ApJS, 247, 69
Eriksson, S. C., Janson, M., & Calissendorff, P. 2019, A&A, 629, A145
Euclid Collaboration, Schirmer, M., Jahnke, K., et al. 2022, A&A, 662, A92
Faherty, J. K., Burgasser, A. J., Cruz, K. L., et al. 2009, AJ, 137, 1
Faherty, J. K., Burgasser, A. J., Walter, F. M., et al. 2012, ApJ, 752, 56
Faherty, J. K., Gagné, J., Popinchalk, M., et al. 2021, ApJ, 923, 48
Faherty, J. K., Rice, E. L., Cruz, K. L., Mamajek, E. E., & Núñez, A. 2013, AJ, 145, 2
Faherty, J. K., Riedel, A. R., Cruz, K. L., et al. 2016, ApJS, 225, 10
Filippazzo, J. C., Rice, E. L., Faherty, J., et al. 2015, ApJ, 810, 158
Gagné, J., Allers, K. N., Theissen, C. A., et al. 2018a, ApJL, 854, L27
Gagné, J., Faherty, J. K., Cruz, K. L., et al. 2015a, ApJS, 219, 33
Gagné, J., Faherty, J. K., Mamajek, E. E., et al. 2017, ApJS, 228, 18
Gagné, J., Fontaine, G., Simon, A., & Faherty, J. K. 2018b, ApJL, 861, L13
Gagné, J., Lafrenière, D., Doyon, R., Malo, L., & Artigau, É. 2014, ApJ, 783, 121
Gagné, J., Lambrides, E., Faherty, J. K., & Simcoe, R. 2015b, FireHose_v2: Firehose v2.0, Zenodo, doi:10.5281/zenodo.18775
Gagné, J., Mamajek, E. E., Malo, L., et al. 2018c, ApJ, 856, 23
Gaia Collaboration, Vallenari, A., Brown, A. G. A., et al. 2023, A&A, 674, A1
Gauza, B., Béjar, V. J. S., Pérez-Garrido, A., et al. 2015, ApJ, 804, 96
Gratton, R., Bonavita, M., Mesa, D., et al. 2024, A&A, 684, A69
Guerra Toro, M. E., Zhou, Y., & Bowler, B. P. 2022, RNAAS, 6, 250
Hiranaka, K., Cruz, K. L., Douglas, S. T., Marley, M. S., & Baldassare, V. F. 2016, ApJ, 830, 96
Hood, C. E., Fortney, J. J., Line, M. R., & Faherty, J. K. 2023, ApJ, 953, 170
Humphreys, A., Schapera, N., Meisner, A. M., et al. 2020, in ASP Conf. Ser. 525, 2020 Compendium of Undergraduate Research in Astronomy and Space Science, ed. J. B. Jensen, J. Barnes, & B. Wardell (San Francisco, CA: ASP), 57
Kausch, W., Noll, S., Smette, A., et al. 2015, A&A, 576, A78
Kellogg, K., Metchev, S., Geißler, K., et al. 2015, AJ, 150, 182
Kirkpatrick, J. D. 2005, ARA&A, 43, 195
Kirkpatrick, J. D., Barman, T. S., Burgasser, A. J., et al. 2006, ApJ, 639, 1120
Kirkpatrick, J. D., Gelino, C. R., Faherty, J. K., et al. 2021, ApJS, 253, 7
Kirkpatrick, J. D., Looper, D. L., Burgasser, A. J., et al. 2010, ApJS, 190, 100
Kirkpatrick, J. D., Marocco, F., Gelino, C. R., et al. 2024, ApJS, 271, 55
Kiwy, F. 2022, unTimely_Catalog_explorer: A Search and Visualization Tool for the unTimely Catalog, Astrophysics Source Code Library, ascl:2211.005
Kuchner, M. J., Faherty, J. K., Schneider, A. C., et al. 2017, ApJL, 841, L19
Laureijs, R., Amiaux, J., Arduini, S., et al. 2011, arXiv:1110.3193
Lawrence, A., Warren, S. J., Almaini, O., et al. 2007, MNRAS, 379, 1599
Lew, B. W. P., Apai, D., Zhou, Y., et al. 2016, ApJL, 829, L32
Linsky, J. L. 1969, ApJ, 156, 989
Liu, M. C., Dupuy, T. J., & Allers, K. N. 2016, ApJ, 833, 96
Liu, M. C., Magnier, E. A., Deacon, N. R., et al. 2013, ApJL, 777, L20
Liu, P., Biller, B. A., Vos, J. M., et al. 2024, MNRAS, 527, 6624
Looper, D. L., Kirkpatrick, J. D., Cutri, R. M., et al. 2008, ApJ, 686, 528
Lucas, P. W., Roche, P. F., Allard, F., & Hauschildt, P. H. 2001, MNRAS, 326, 695
Malo, L., Doyon, R., Lafrenière, D., et al. 2013, ApJ, 762, 88
Manjavacas, E., Karalidi, T., Vos, J. M., Biller, B. A., & Lew, B. W. P. 2021, AJ, 162, 179
Marley, M. S., Saumon, D., & Goldblatt, C. 2010, ApJL, 723, L117
Marley, M. S., Saumon, D., Visscher, C., et al. 2021, ApJ, 920, 85
Marocco, F., Day-Jones, A. C., Lucas, P. W., et al. 2014, MNRAS, 439, 372
Marocco, F., Eisenhardt, P. R. M., Fowler, J. W., et al. 2021, ApJS, 253, 8
Marois, C., Macintosh, B., Barman, T., et al. 2008, Sci, 322, 1348
Marois, Christian, Zuckerman, B., Konopacky, Quinn M., et al. 2010, Natur, 468, 1080
Martin, E. C., Mace, G. N., McLean, I. S., et al. 2017, ApJ, 838, 73
McCarthy, A. M., Muirhead, P. S., Tamburo, P., et al. 2024, ApJ, 965, 83
McGovern, M. R., Kirkpatrick, J. D., McLean, I. S., et al. 2004, ApJ, 600, 1020
McMahon, R. G., Banerji, M., Gonzalez, E., et al. 2013, Msngr, 154, 35
Meisner, A. M., Caselden, D., Schlafly, E. F., & Kiwy, F. 2023, AJ, 165, 36
Metchev, S. A., Heinze, A., Apai, D., et al. 2015, ApJ, 799, 154
Miles, B. E., Biller, B. A., Patapis, P., et al. 2023, ApJL, 946, L6
Miles, B. E., Skemer, A. J., Barman, T. S., Allers, K. N., & Stone, J. M. 2018, ApJ, 869, 18
Miles-Páez, P. A., Metchev, S., Apai, D., et al. 2019, ApJ, 883, 181
Morley, C. V., Mukherjee, S., Marley, M. S., et al. 2024, arXiv:2402.00758
Piscarreta, L., Mužić, K., Almendros-Abad, V., et al. 2024, A&A, 686, A37
Plummer, M. K., Wang, J., Artigau, É., Doyon, R., & Suárez, G. 2024, arXiv:2403.04840
Radigan, J. 2014, ApJ, 797, 120
Radigan, J., Jayawardhana, R., Lafrenière, D., et al. 2012, ApJ, 750, 105
Rodrigo, C., & Solano, E. 2020, in XIV.0 Scientific Meeting (virtual) of the Spanish Astronomical Society (Madrid: La Sociedad Española de Astronomía), 182, https://www.sea-astronomia.es/reunion-cientifica-2020
Rodrigo, C., Solano, E., & Bayo, A. 2012, IVOA Working Draft 1015
Sanghi, A., Liu, M. C., Best, W. M. J., et al. 2023, ApJ, 959, 63
Schneider, A. C., Burgasser, A. J., Bruursema, J., et al. 2023a, ApJL, 943, L16
Schneider, A. C., Cushing, M. C., Kirkpatrick, J. D., et al. 2014, AJ, 147, 34
Schneider, A. C., Hardegree-Ullman, K. K., Cushing, M. C., Kirkpatrick, J. D., & Shkolnik, E. L. 2018, AJ, 155, 238
Schneider, A. C., Munn, J. A., Vrba, F. J., et al. 2023b, AJ, 166, 103
Schneider, A. C., Windsor, J., Cushing, M. C., Kirkpatrick, J. D., & Wright, E. L. 2016, ApJL, 822, L1
Schneider, A. C., Windsor, J., Cushing, M. C., Kirkpatrick, J. D., & Shkolnik, E. L. 2017, AJ, 153, 196
Shkolnik, E. L., Allers, K. N., Kraus, A. L., Liu, M. C., & Flagg, L. 2017, AJ, 154, 69
Showman, A. P., & Kaspi, Y. 2013, ApJ, 776, 85
Simcoe, R. A., Burgasser, A. J., Schechter, P. L., et al. 2013, PASP, 125, 270
Skrutskie, M. F., Cutri, R. M., Stiening, R., et al. 2006, AJ, 131, 1163
Spiegel, D. S., Burrows, A., & Milsom, J. A. 2011, ApJ, 727, 57
Suárez, G., & Metchev, S. 2022, MNRAS, 513, 5701
Suárez, G., & Metchev, S. 2023, MNRAS, 523, 4739
Suárez, G., Metchev, S., Leggett, S. K., Saumon, D., & Marley, M. S. 2021, ApJ, 920, 99
Suárez, G., Vos, J. M., Metchev, S., Faherty, J. K., & Cruz, K. 2023, ApJL, 954, L6

Tannock, M. E., Metchev, S., Heinze, A., et al. 2021, AJ, 161, 224
Torres, C. A. O., Quast, G. R., Melo, C. H. F., & Sterzik, M. F. 2008, in Handbook of Star Forming Regions, Volume II: The Southern Sky, ed. B. Reipurth, Vol. 5 (San Francisco, CA: ASP), 757
Vacca, W. D., Cushing, M. C., & Rayner, J. T. 2003, PASP, 115, 389
Viana Almeida, P., Santos, N. C., Melo, C., et al. 2009, A&A, 501, 965
Vos, J. M., Allers, K. N., & Biller, B. A. 2017, ApJ, 842, 78
Vos, J. M., Allers, K. N., Biller, B. A., et al. 2018, MNRAS, 474, 1041
Vos, J. M., Biller, B. A., Allers, K. N., et al. 2020, AJ, 160, 38
Vos, J. M., Biller, B. A., Bonavita, M., et al. 2019, MNRAS, 483, 480
Vos, J. M., Burningham, B., Faherty, J. K., et al. 2023, ApJ, 944, 138
Vos, J. M., Faherty, J. K., Gagné, J., et al. 2022, ApJ, 924, 68
Whiteford, N., Glasse, A., Chubb, K. L., et al. 2023, MNRAS, 525, 1375
Yang, H., Apai, D., Marley, M. S., et al. 2016, ApJ, 826, 8
Zhou, Y., Bowler, B. P., Apai, D., et al. 2022, AJ, 164, 239
Zhou, Y., Bowler, B. P., Morley, C. V., et al. 2020, AJ, 160, 77
Zuckerman, B. 2019, ApJ, 870, 27
Zuckerman, B., & Song, I. 2004, ARA&A, 42, 685
Zuckerman, B., Song, I., Bessell, M. S., & Webb, R. A. 2001, ApJL, 562, L87
Zuckerman, B., Song, I., & Bessell, M. S. 2004, ApJL, 613, L65